

Planning Grasps for Assembly Tasks

Weiwei Wan, *Member, IEEE*, Kensuke Harada, *Member, IEEE*, and Fumio Kanehiro, *Member, IEEE*

Abstract—This paper develops model-based grasp planning algorithms for assembly tasks. It focuses on industrial end-effectors like grippers and suction cups, and plans grasp configurations considering CAD models of target objects. The developed algorithms are able to stably plan a large number of high-quality grasps, with high precision and little dependency on the quality of CAD models. The undergoing core technique is superimposed segmentation, which pre-processes a mesh model by peeling it into facets. The algorithms use superimposed segments to locate contact points and parallel facets, and synthesize grasp poses for popular industrial end-effectors. Several tunable parameters were prepared to adapt the algorithms to meet various requirements. The experimental section demonstrates the advantages of the algorithms by analyzing the cost and stability of the algorithms, the precision of the planned grasps, and the tunable parameters with both simulations and real-world experiments. Also, some examples of robotic assembly systems using the proposed algorithms are presented to demonstrate the efficacy.

Index Terms—Grasp synthesis, Grasp planning, Regrasp

I. INTRODUCTION

THIS paper develops algorithms to automatically plan grasping poses for assembly tasks. It focuses on industrial end-effectors, and plans grasp configurations for these end-effectors considering CAD models of target objects.

Developing grasp planning algorithms is important to manufacturing using “teachingless” robotic manipulators. Modern robotic manipulation systems use manually annotated or pre-taught grasp configurations to perform certain tasks, which is not only costly but also difficult to redeploy. Automatic grasp synthesis or planning algorithms could bypass the annoying manual work and enable fast redeployment for varying and changing manufacture. For this reason, lots of studies in the field of robotic grasp have been devoted to automatic grasp planning and many grasp planning algorithms have been developed. These algorithms are able to plan grasps considering forces and collisions. However, they hardly meet the requirements of fully automatic manufacturing applications like bin-picking and assembly. The requirements include but are not limited to: (1) Large number of candidate grasps: The grasp planner is expected to provide a large number of candidate grasp poses for optimization. (2) Stableness: The grasp planner must have little dependency on the quality of CAD models. (3) Precision: Object poses do not change much after being grasped by the planned grasps.

On the other hand, state-of-the-art grasp planning studies concentrate on theoretical aspects like grasp closures and qualities, or applicational aspects like grasping using multi-finger hands, dexterous hands, and hands with tactile and force sensors. Grasp planning for popular industrial end-effectors,

e.g. parallel grippers and suction cups, is usually ignored since grasping rigid objects using suction cups and parallel grippers is considered to be easy and solved. In this paper, we reinspect this opinion and restudy the grasp planning problem for parallel grippers. After reviewing previous work, we found that although grasp planner for parallel grippers had existed for decades, they do not really meet the requirements of industrial tasks: Some old-fashioned algorithms could plan grasps for simple polytopes, but they cannot tackle complicated mesh models and output satisfying number of grasps; Modern grasp planning algorithms aim to find stable grasps. They cannot find a large amount of grasping poses and don’t consider about their precision. It is difficult to use the planned grasps for industrial tasks like bin-picking and assembly, etc.

Under this background, this paper develops new grasp planning algorithms for industrial bin picking and assembly. The problem setting is formulated as follows. The input includes: (1) Kinematic models of industrial end-effectors like suction cups, parallel grippers, and three-finger-one-parameter grippers; (2) Water-tight models of rigid objects. The output is: A set of automatically planned grasp configurations. The algorithms assume: (1) The objects have rigid bodies. Soft or changeable objects are not considered; (2) The end-effectors and manipulators are actuated using position control to ensure fast operation. Tactile or F/T sensors are not available.

The undergoing core technique of the developed algorithms is superimposed segmentation. The algorithms pre-process a mesh model by peeling it into facets. Each facet is allowed to overlap with others and is thus called superimposed segmentation. The overlap and sizes of segments are controlled by several tunable parameters, which allow users to change the quality of planned grasps following the requirements of their applications. The superimposed segments are used to determine contact and compute parallel facets. Grasp poses for popular industrial end-effectors are planned considering the contact and parallel facets.

The developed algorithms could plan a large number of precise grasps with little dependency on the quality of CAD models. Object positions change less than $2mm$ after being grasped the planned grasps. The computational cost and the stability of the algorithms in the presence of low-quality CAD models, as well as the number of planned grasps and their precision are analyzed in detail in the experimental section using both simulational and real-world experiments. The effect of the tunable parameters is analyzed by comparing the results of varying values. A real dual-arm regrasp and assembly system is also implemented to show the efficacy of the proposed algorithms.

The rest of the paper is organized as follows. Section II reviews related work. Section III discusses the fundamental technique like superimposed segmentation and sampling

Weiwei Wan and Kensuke Harada are with Graduate School of Engineering Science, Osaka University, Japan. Fumio Kanehiro is with National Inst. of AIST, Japan. E-mail: wan@sys.es.osaka-u.ac.jp

contact points. Section IV presents details of grasp planning algorithms using the fundamental technique. Section V is the experimental section. Section VI draws conclusions.

II. RELATED WORK

This paper develops model-based grasp planning algorithms for suction cups and parallel grippers. Accordingly, this section reviews related studies on grasp theories and grasp planning of suction cups and parallel grippers, with a special focus on the preprocessing of mesh models.

A. Grasp theories and grasp planning

Grasp theories study form/force closure and closure qualities. The theoretical studies are applicable to suction cups, parallel grippers, as well as other robotic hands. Some early work like [1][2] studied point fingers and polygonal objects, with later extensions to more realistic scenarios like curved surfaces and fingers [3][4][5][6][7], considering grasp stability [8][9][10] and grasp metrics [11][12]. The early theoretical studies were mostly 2D, and the concentration was to estimate the stability of grasps and the resistance to external wrenches. The theoretical studies were extended to 3D polyhedral objects or mesh models composed of flat faces later, assuming to be hard point contacts. Examples include [13], [14], etc. Some other studies optimized the planned grasps [15] using some quality metrics [16].

Planning grasp poses for real-world objects and real-world end-effectors are more challenging than the early theoretical studies. There is a big gap between the computed results and real-world executions. One has to consider many factors like contact regions, object surface curvatures, resistance to torque caused by gravity forces, kinematics of robot hands, etc., to secure stable and exact grasps. Several previous studies challenged these difficulties. For example, Wolter et al. [17] considered the geometry of grippers during the automatic generation of grasps for 3D rectilinear objects. Jones et al. [18] considered the parallel faces of a 3D object as well as the mesh model of a robot gripper to plan two finger grasps for pick-and-place operations. Liu et al. [19] used the attractive regions of an object to plan stable grasps. Pozzi et al. [20] discussed grasp qualities considering the kinematic structures of underactuated and compliant hands. Shi et al. [21] considered about environmental constraints as well as the kinematic constraints of robot hands to plan accessible grasps for bin-picking and kitting tasks. Li et al. [22] used stretching ropes (cord geometry) to find the contact of a hand jaw with object surfaces and hence plan the grasps. Ciocarlie et al. [23] considered about local geometry and structures at contact points and modeled friction forces using soft models. Harada et al. [24] discussed about a gripper with soft finger pads attached to the finger tips and analyzed object mesh models considering the depth of contacts. These studies used gripper models and their kinematic structures to ensure feasibility, and considered about contact properties by analyzing the meshes around contact regions.

Our work plans grasp for suction cups and parallel grippers. For these simple end-effectors, the form/force closure theory

is converted to comparing surface normals at the contacts. The kinematic constraints, contact, and quality of grasps are considered in segmentation, sampling, and nested collision detection. The quality of the planned grasps depends on the preprocessing of mesh models, which is further reviewed below.

B. Preprocessing mesh models

Two major approaches to preprocess the mesh models for grasp planning are (1) primitive fitting and (2) surface segmentation. The first approach represents mesh models using a set of shape primitives, and plans grasp by considering the fitting errors or using pre-annotated grasps. The second approach represents mesh models using coplanar triangle sets. Each coplanar segmented triangle set is named a facet and equals to one constitutional polygon of a polyhedron.

For primitive fitting-based grasp planning, Goldfeder et al. [25] represented a mesh model using recursive splitting and fitting of primitive superquadrics [26]. El-Khoury et al. [27] fitted segmented point clouds using primitive superquadrics and used pre-annotated training sets to learn grasp points from the fitted models. Xue et al. [28] also used primitive superquadrics to fit models and plan grasps for Schunk Anthropomorph Hands. Other than superquadrics-based fitting, Miller et al. [29] represented a mesh model using a set of primitive mesh models like boxes and spheres, and use a set of rules defined on the primitives to generate grasps for the mesh model. Hueber et al. [30] fitted mesh models using different levels of primitive boxes and planned grasp by evaluating the annotated grasps on the primitives. Bonilla et al. [31] also fitted mesh models using primitive boxes, and planned grasps using geometric information extracted from the primitive boxes. Nagata et al. [32] proposed an interactive method for grasp planning by assuming shape primitives. Yamanobe et al. [33] defined the gripping configurations of several shape primitives and used primitive shape representation to planning grasps for mobile manipulators. Curtis et al. [34] used primitives to learn grasps. Instead of explicitly fitting primitives, the authors used learned grasping knowledge on a set of primitive objects to speed up the process of planning successful grasps for novel objects. Harada et al. [35] used cylinders to fit banana point clouds, and planned robust grasps by analyzing the projections of the point clouds on the cylindrical axes denoted by the fitted cylinders. The grasp moduli space proposed by Porkorny et al. [36] is also a primitive fitting approach. The primitive fitting approaches do not assure the stability of planned grasps and exact object poses after grasping. Some further evaluations or optimizations are needed to make the results practical.

For surface segmentation-based grasp planning, Harada et al. [24] clustered triangle meshes by using a parameter denoting softness of contacts and implemented grasp planning for grippers with soft finger pads. Tsuji et al. [37] used multi-level clustering [38] to find the concavity and convexity of mesh models, and used stress distribution models to plan stable grasps. Hang et al. [39] also used multi-level clustering to plan grasps. The difference is their goal was not to find grasping features. Instead, they use different levels of simplification

for iterative searching of stable grasps under reachability constraints. In a later work, Hang et al. [40] extended the study to fingertip spaces and used multi-resolution contacts to expedite grasp synthesis. The results of the multi-level planning were demonstrated in [41] using an Allegro hand. The hand could gait to different configurations as the weights of objects change. Some of the primitive fitting approaches also have a segmentation step, where meshes or point clouds are segmented for fitting [27][42].

The algorithms developed in this paper use surface segmentation to plan contacts and estimate closure qualities. Unlike previous work which segmented each triangle into a single facet or performed multi-level segmentation, the algorithms allow superimposed segmentation. Each triangle is repeatedly segmented into different facets, and the overlap and thickness of facets are controlled by tunable parameters pertaining to surface normals. By using sampled contact regions on the superimposed segmentations and leveraging torque resistance, one may automatically plan a large number of stable and precise grasp configurations for suction cups and parallel grippers.

III. PRE-PROCESSING MESH MODELS

A. Superimposed segmentation

Superimposed segmentation provides uniform facets. Conventional approaches [38][43] cluster each triangle into a single facet, resulting in uneven facets – Some of them could be very large, while others are very small. Unlike the conventional approaches, superimposed segmentation allows one triangle to be repeatedly clustered to multiple facets, making all facets uniform (equally large). The clustered facets do not exclusively occupy the triangles that might also belong to other facets.

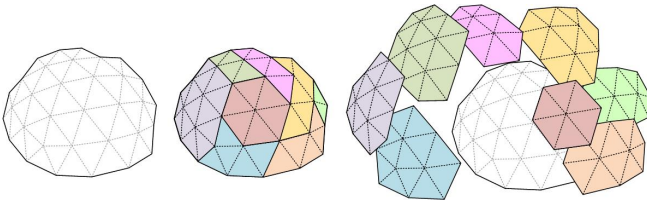


Fig. 1: Segmenting mesh models into superimposed facets. Left: Original mesh model. Middle: Results of segmentation. Right: The facets are superimposed.

The superimposed segmentation is computed as follows. First, the algorithm initiates a seed triangle and scans the surrounding triangles of the seed. See the left part of Fig.2 for example. The purple triangle is the seed triangle, and the algorithm scans the triangles surrounding it. If the angle between the normal of the seed triangle and the normal of a nearby triangle is smaller than a threshold θ_{pln} , the adjacent triangle is clustered into the same facet as the seed triangle. In the figure, the angles between the black arrows and the purple arrow are equal to or smaller than θ_{pln} , the related triangles are clustered into the purple facet. In contrast, the angles between the grey arrows and the purple arrow are larger than θ_{pln} , the related triangles are not included. θ_{pln} is a tunable parameter which controls the planarity of a facet.

After clustering the first facet, the algorithm initiates a new seed triangle and repeats the clustering by starting from the new seed. The routine to initiate a new seed is as follows. The algorithm scans the surrounding triangles of the previous seeds and checks the angles between the normals of the previous seeds and the normals of the surrounding triangles. If an angle is larger than θ_{fct} , the related triangle is selected as the new seed. The right part of Fig.2 shows an example. The angle between the green normal and the purple normal is larger than θ_{fct} . Thus, the green the triangle with the green normal is selected as the new seed. The algorithm repeats the clustering process by using new seed and generates a new facet (the green facet shown in the right part of Fig.2). θ_{fct} is a tunable parameter which controls the superimposition of facets.

During clustering, all triangles are repeatedly scanned, which allows one triangle to be clustered into multiple facets. The facets could superimpose with each other. On the other hand, the normals of all previous seeds are compared when initiating a new seed, which ensures each facet to be unique and the algorithm to stop properly.

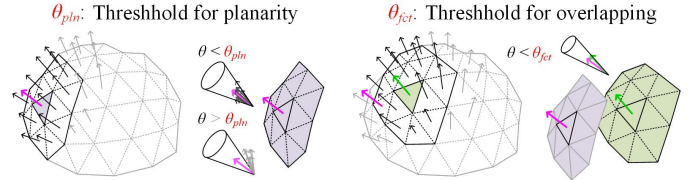


Fig. 2: The superimposition is controlled by two parameters. (1) θ_{pln} controls planarity of each facet. (2) θ_{fct} controls the overlap of facets.

B. Sampling contact points

1) *Sampling and distributing*: Contact points are computed by sampling the surface of the object mesh model. The sampling is performed over the whole surface to provide evenly distributed contact points on the mesh. After sampling, the sampled points are repeatedly distributed to the superimposed facets as their contact points. Note that we avoided sampling individual facets since it only provides evenly distributed contact points on individual facets, the overall distribution relies on segmenting methods. In cases where facets are small, individual sampling may fail to produce contact points.

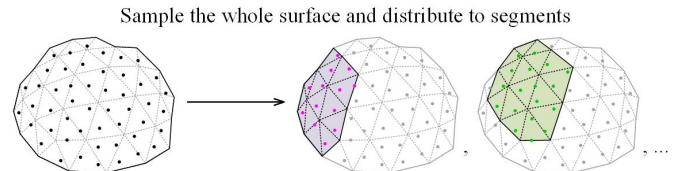


Fig. 3: Left: Sample over the whole mesh surface. Right: Distribute the samples to each facet to avoid repeated sampling.

Take Fig.3 for example. In the left part, the whole mesh surface is sampled. In the right part, the sampled points are distributed to superimposed facets. The surface is sampled once and the sampled points are distributed to individual

facets repeatedly. The method ensures the contact points on each facet have equal density and are evenly distributed. It is irrelevant to the segmentation methods. Also, the method distributes the samples to multiple facets without sampling again. It avoids repeated computation and improves algorithm efficiency.

2) *Removing bad samples*: The output of sampling and distributing cannot be used directly, since the distributed samples might be (1) near the boundary of facets and (2) near to each other. In the first case, attaching fingerpads to the sampled points near facet boundaries lead to unstable grasps. In the second case, attaching fingerpads to the near points produces similar grasping configurations, which results in a large number of similar grasps and is wasteful. To avoid the problems, we perform two refining processes where the first one computes the distance between a contact point and the boundary of its facet. The points with distances smaller than t_{bdry} will be removed. The second one removes the contact points that are too close to others. The remaining contact points after being refined by the first process are further screened using the Radius Nearest Neighbour (RNN) algorithm to remove nearby points with a distance smaller than t_{rnn} . Like θ_{pln} and θ_{fct} , t_{bdry} and t_{rnn} are tunable parameters of the grasp planner.

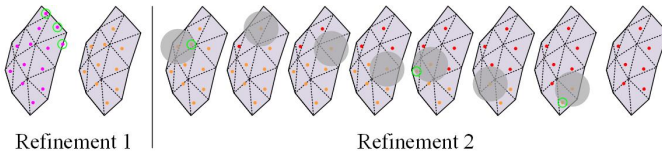


Fig. 4: Two refinements that remove the bad contact points. The first refinement removes the contact points with small distances to facet boundaries. The second refinement removes the contact points that are too close to others.

In practice, t_{rnn} is determined by the size of finger pads. An end-effector contacts with objects at a region, instead of a single point. t_{rnn} specifies the radius of the contact region. It controls the density of planned grasps by removing nearby candidates.

As a demonstration, Fig.5 shows the process of sampling contact points using a plastic workpiece shown in Fig.5(a).

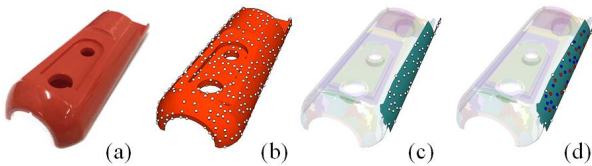


Fig. 5: Sampling contact points. (a) The original object. (b) The sampled contact points. (c) The contact points distributed to one facet. (d) Removing bad contact points. Especially in (d), the white points are removed since they are too near to the boundary. The red points are the results of RNN screening.

3) *Stability*: The Soft-Finger Contact (SFC) model proposed in [44] is used to estimate the stability of a grasp. The

force and torque exerted by one SFC is expressed as:

$$\mathbf{f}_t^T \mathbf{f}_t + \frac{\tau_n^2}{e_n^2} \leq \mu^2 f_n^2 \quad (1)$$

Here, \mathbf{f}_t indicates the tangential force at the contact. τ_n^2 indicates the torque at the contact. f_n indicates the load applied in the direction of the contact normal. e_n is the eccentricity parameter which captures the relationship between maximum frictional force and moment. Under the Winler elastic foundation model, e_n is

$$e_n = \frac{\max(\tau_n)}{\max(f_t)} = \frac{\int_S r \mu K u_i(r) dS}{\int_S \mu K u_i(r) dS} \quad (2)$$

where K is the elastic modulus of the foundation over the thickness of the soft finger pad. S is the contact surface between the finger pad and the object. r is the distance between a differential contact point and the center of the contact region. $u_i(r)$ is the depth of the soft penetration. These symbols are illustrated in Fig.6.

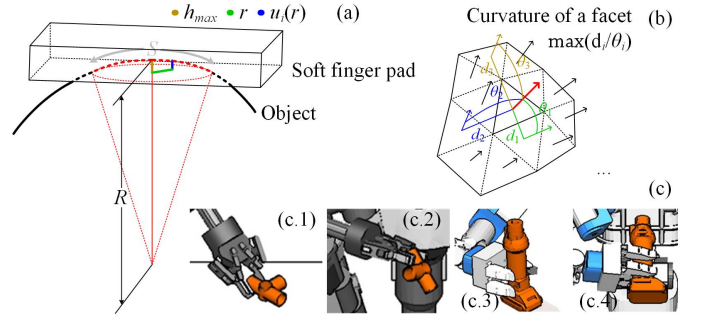


Fig. 6: (a) The soft finger contact model. (b) Curvature of a facet. (c) The goal is to make sure the object is stable at an arbitrary pose.

Using R to denote the radius of the the contact curvature, $u_i(r)$ can be represented by

$$u_i(r) = \sqrt{R^2 - r^2} - (R - h_{max}) \quad (3)$$

where h_{max} is the maximum depth of the soft penetration. Following the definition of curvature, R could be computed using $\max(d_i/\theta_i)$, where d_i is the distance between the center of the i th in the facet and the center of the seed triangle, θ_i is the angle between the normal of the i th triangle and the normal of the seed triangle. The computation is illustrated in Fig.6(b). R is essentially determined by the geometry of a facet. h_{max} is used as a tunable parameter to control the stability of planned grasps. Since the goal of stability estimation is to make sure the object is stable at an arbitrary pose (Fig.6(c)), a planned grasp must meet¹

$$(mgc)^2 \leq e_n^2 (\mu^2 f_n^2 - (mg)^2) \quad (4)$$

¹Here, we are considering the worst case where the gripping torque must resist the largest torque caused by gravity. During manipulation, the largest external torque appears when gravity direction is perpendicular to vector $\text{contact} - \text{com}$.

where c is the distance between the *com* (center of mass) of the object and the center of contacts. From (2), (3), and (4) we obtain

$$(mgc)^2 \leq \left(\frac{8}{15}\right)^2 (2Rh_{max} - h_{max}^2)(\mu^2 f_n^2 - (mg)^2) \quad (5)$$

This equation is used to determine the stability of planned grasps.

IV. PLANNING THE GRASP CONFIGURATIONS

Using the superimposed facets and the sampled contact points, we develop algorithms to plan grasps for suction cups and parallel grippers.

A. Suction cups

We assume a suction end-effector has only one suction cup. The grasp planning algorithm for a single suction cup is a two-step process. In the first step, the algorithm finds the possible orientations to attach the suction cup to the sampled and refined contact points. Since the approaching direction must be perpendicular to the contact region, the end-effector's orientation is only changeable by rotating around the approaching direction. The algorithm poses the suction cup to the contact points from the changeable orientations and removes the infeasible (collided) grasps. In the second step, the algorithm examines the resistance of planned suction configurations to external torques caused by gravity. The pseudocode of the algorithm is shown in Fig.7.

```

1  plannedgrasps=[]
2  for each contact, contactnormal in facet:
3    for theta in discreteangles:
4      /* size(discreteangles) =  $n_{da}$  */
5      rotmat = rodrigues(contactnormal, theta)
6      eemesh.setpose(contact, rotmat)
7      if checkcollision(eemesh, objmesh) is False:
8        if checktorque(contact, objcom, hmax)
9          plannedgrasps.add([contact, rotmat])

```

Orientation and collision

Fig. 7: The pseudocode of grasp planning for suction cups. It is a two step process where the first step finds possible orientations and performs *checkcollision*, the second step performs *checktorque*.

For each contact point, the algorithm discretizes the rotation around the contact normal into *discreteangles*, and computes the rotation matrices. The number of discretized values is determined by n_{da} . The algorithm poses the *eemesh* (mesh model of the end effector) using the computed rotation matrices and checks the collision between the *eemesh* and the *objmesh* (mesh model of the object). Line 3 of the pseudocode iterates through the discrete orientations. Line 6 poses the *eemesh* to a *contact* with rotation matrix *rotmat*. Line 7 checks the collision between *eemesh* and *objmesh*.

In the second step, the algorithm further examines the resistance to external torques. The function *checktorque*(*contact*, *objcom*, *h_{max}*) in line 8 of the pseudocode performs the

examination. The function computes the Euclidean distance between *contact* and *objcom* (the *com* of the object), and checks if Eq.(4) is met.

Fig.8 shows the results of grasp planning for a suction cup and a metal workpiece. A single grasp is shown in Fig.8(a). All planned results are shown in Fig.8(b). The red configurations in Fig.8(b) are the grasps deleted by the *checkcollision*(*eemesh*, *objmesh*) function.

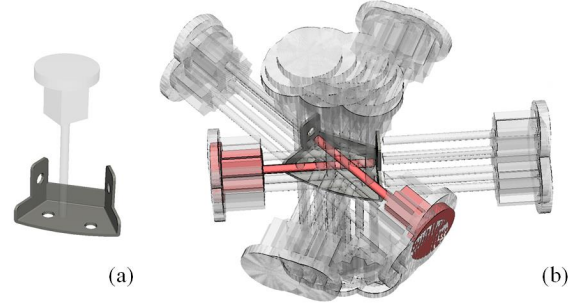


Fig. 8: Results of grasp planning for a suction cup and a metal workpiece. (a) One of the planned grasps. (b) All results. The red grasps collide with the metal workpiece.

B. Two-finger parallel grippers

Grasp planning for two-finger parallel grippers is a three-step process. In the first step, the planner for two-finger parallel grippers first finds parallel facets and computes candidate contact pairs by examining the contact points on the parallel facets. Compared with suction cups which need one contact point, the planner for two-finger parallel grippers needs two contact points with opposite contact normals. Thus, the algorithm involves an extra step to prepare the candidate contact pairs. The second and third steps are similar to suction cups. In step two, the algorithm finds the possible orientations to attach the parallel gripper to the candidate contact pairs. In step three, the algorithm examines the stability of the planned grasps.

The pseudocode of the grasp planner for two-finger parallel grippers is shown in Fig.9. In the first block (lines 1 to 8), the algorithm finds candidate contact pairs. For each pair of parallel facets, the algorithm initiates a ray that starts from a contact point on one facet and points to the inverse direction of the contact normal. It detects the intersection between the ray and the other facet. If an intersection exists, the contact-intersection pair is saved as a candidate. Whether two facets in a pair are parallel is determined by a tunable parameter θ_{part} (see line 3). In the second block (lines 10 to 22), the algorithm performs collision detection and examines stability. The algorithm invokes two nested *checkcollision* functions in the second block. In the first call (line 14), the algorithm checks if the stroke of the gripper collides with the object. Stroke is represented by cylinders which do not have orientation. In the second call (line 20), the algorithm checks if the whole hand (both fingers and palm) collides with the object. The algorithm poses the fingertips to the center of the contact pairs and performs collision at different

rotations around the axis formed by the two contacts. During the process, the planner attaches one finger pad to one position of a contact pair, and attaches the other finger pad to the other position of the contact pair. Suppose the two parallel fingers are f_1, f_2 , the contact pair is $[contact_a, contact_b]$, the algorithm attaches f_1 to $contact_a$, attaches f_2 to $contact_b$, rotates the gripper around the axis $contact_a - contact_b$, and checks the collision between $eemesh$ and $objmesh$ at every orientation (lines 15 to 20).

```

1  candidatepairs = []
2  for each pair (faceta, facetb) in objmesh:
3    if dot(segmentnormala, segmentnormalb) < cos( $\theta_{par}$ ):
4      for each contacta, contactnormala on segmenta:
5        ray = ray(contacta, -contactnormala)
6        contactb = intersect(ray, segmentb)
7        if contactb is not None:
8          candidatepairs.add([contacta, contactb])
9
10 plannedgrasps = []
11 for each pair (contacta, contactb) in candidatepairs:
12   stmesh.setpose(contacta, contactnormala,
13                 contactb, contactnormalb)
14   if checkcollision(stmesh, objmesh) is False:
15     for theta in discreteangles:
16       /* size(discreteangles) =  $n_{da}$  */
17       tipposition = (contacta + contactb) / 2
18       rotmat = rodrigues(contacta - contactb, theta)
19       eemesh.setpose(tipposition, rotmat)
20       if checkcollision(eemesh, objmesh) is False:
21         if checktorque(tipposition, objcom,  $h_{max}$ )
22           plannedgrasps.add(
                [contacta, contactb, rotmat])

```

Fig. 9: Pseudocode of grasp planning for two-finger parallel grippers. $stmesh$ denotes the collision model of a gripper's stroke. $eemesh$ denotes the collision model of a gripper.

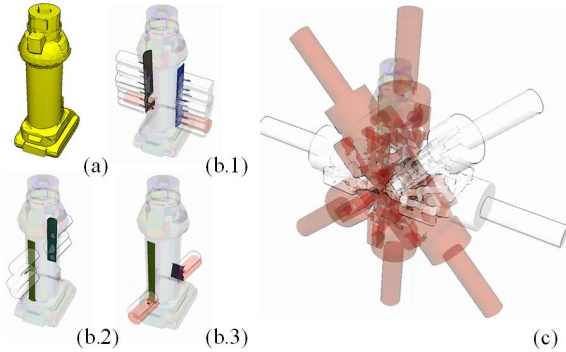


Fig. 10: Results of grasp planning for a Robotiq85 gripper and an electric drill. (a) The CAD model of the drill. (b.1-3) Some of the parallel facets and the results of $checkcollision(stmesh, objmesh)$. The cylinders indicate the stroke of the gripper. The red ones collide with the drill. The white ones are collision-free. (b) The discretized grasps at one contact pair. The red hands indicate the obstructed grasps. The white ones are the planned grasps.

Fig.10 shows the results of grasp planning for a Robotiq85 gripper and an electric drill. The CAD model of the drill is shown in Fig.10(a). The collision between strokes and the model is detected at line 14 of Fig.9. Fig.10(b.1-3) draw some results of the collision detection. The red cylinders show the strokes that collide with the object and are removed to avoid repeated collision checking at different orientations. The white cylinders are further examined in line 20 of Fig.9 to see if there is a collision between the whole hand and the object. The discretized orientations at one contact pair and the results of whole-hand collision detection are illustrated in Fig.10(c). The red hands indicate the collided grasps found by $checkcollision(eemesh, objmesh)$. The white ones are the planned grasps.

C. Three-finger parallel grippers

In addition, the planner proposed in this paper is applicable to three-finger parallel grippers where two fingers are actuated together against a third finger.

```

1  plannedgrasps = []
2  for each pair (contacta, contactb) in candidatepairs:
3    for theta in discreteangles:
4      /* size(discreteangles) =  $n_{da}$  */
5      tipposition = (contacta + contactb) / 2
6      rotmat = rodrigues(contacta - contactb, theta)
7      stmesh.setpose(tipposition, rotmat)
8      if checkcollision(stmesh, objmesh) is False:
9        eemesh.setpose(tipposition, rotmat)
10       if dist( $f_2$ , objmesh) <  $l_{dct}$  and dist( $f_3$ , objmesh) <  $l_{dct}$ 
11         if checkcollision(eemesh, objmesh) is False:
12           if checktorque(tipposition, objcom,  $h_{max}$ )
13             plannedgrasps.add(
                    [contacta, contactb, rotmat])

```

Fig. 11: Pseudocode of grasp planning for three-finger parallel grippers.

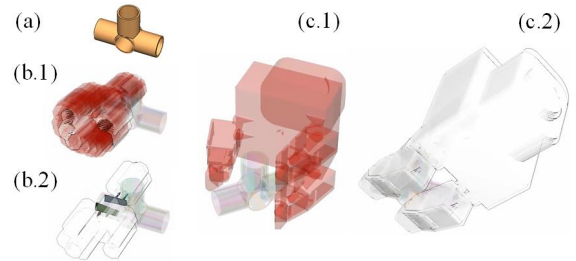


Fig. 12: Results of grasp planning for a three-finger gripper and a tube connector. (a) Mesh model of the object. (b.1) Results of the collision detection on strokes. (b.2) A clear view of the collision-free strokes of (b.1). (c.1) A collided grasp configuration found by the second collision checking. (c.2) A collision-free grasp configuration (it is also one planned grasp configuration).

The process is similar to grasp planning for two-finger parallel grippers, except that the two fingers on one side of the

parallel gripper are treated as a single finger. Its pseudocode is shown in Fig.11. In the first step, the planner finds parallel facets and computes candidate contact pairs (not shown in Fig.11). In the second step, the planner poses the fingertips to the center of the contact pairs and performs collision detection at different rotations around the axis formed by the two contacts (Fig.11). The algorithm also invokes two nested `checkcollision` functions. The first invocation checks the collision of strokes (line 8). The second invocation checks the collision of the whole hand (line 11). However, different from the two-finger case, the stroke of a three-finger gripper is represented by three cylinders, which changes with hand orientation. Thus, both the two invocations are performed under a specific orientation (both are invoked inside the initialized by line 3). If the stroke is collision free, the planner attaches one finger pad to one position of a contact pair and attaches the center of the other two finger pads to the other position of the contact pair (line 9). Suppose the three fingers are f_1 , f_2 , and f_3 where f_1 is at one side of a parallel gripper, f_2 and f_3 are on the other side. The contact pair is named $[contact_a, contact_b]$. The algorithm attaches f_1 to $contact_a$, attaches $\frac{f_2+f_3}{2}$ to $contact_b$, and examines the distances between f_2 and $objmesh$, and f_3 and $objmesh$ (line 9). The algorithm requires $\|f_2-objmesh\| < t_{dct}$ and $\|f_3-objmesh\| < t_{dct}$ where t_{dct} is a tunable parameter. The parameter controls the contact between the two fingers and the object surface. If the distances meet the requirements, the algorithm checks the collision between the gripper and the object (line 10). In the third step, the algorithm examines the stability (line 12).

Fig.12 shows the results of grasp planning for a three-finger gripper and a tube connector. Some exemplary results of collision detection with strokes are illustrated in Fig.12(b.1-b.2). Fig.12(b.1) shows both the collided (red) and collision-free (white) strokes. The two-finger side is in the front. The strokes are rotated around the axis passing through the contact pair. Fig.12(b.2) is a clear view without the collided ones. The collision-free strokes are further examined in the second collision detection. Some exemplary results are illustrated in Fig.12(c.1) (a collided grasp configuration) and Fig.12(c.2) (a collision-free grasp configuration).

V. ANALYSIS AND DEMONSTRATIONS

A. Tunable parameters

In the algorithms, seven tunable parameters are prepared for user configuration. The parameters and their functions are shown in Table.I. This section analyzes the parameters and compares the performance of different parameter settings by comparing the different planned results. In practice, users may set the parameters according to the needs of their robotic systems.

Parameter 1: θ_{pln} is used to control the planarity of each facet during the superimposed segmentation. Smaller θ_{pln} leads to flatter and smaller facets. Fig.13(a) shows the segmented results of the electric drill shown in Fig.10(a) using different θ_{pln} . The facets are drawn with random offsets from their original position to give a clear view. Each facet is given a random color. As θ_{pln} becomes smaller, facets become flatter

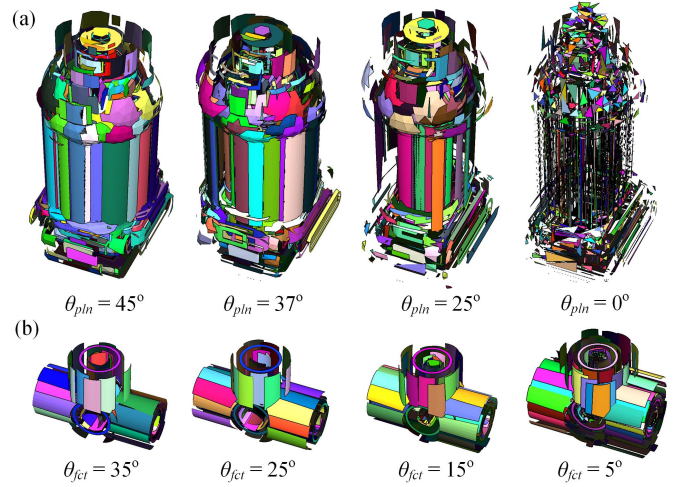


Fig. 13: (a) Results of superimposed segmentation using different θ_{pln} . Each segment is shown in a random color, and is drawn with a random offset from its original position to give a clear view. The results show that a smaller θ_{pln} leads to flatter and smaller facets. (b) Results of superimposed segmentation using different θ_{fct} . The object used for demonstration is the one in Fig.12(a). The results show that a smaller θ_{fct} leads to more overlap.

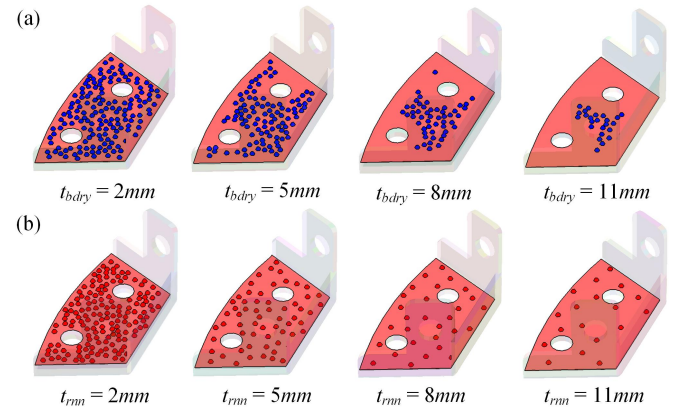


Fig. 14: (a) Results of contact sampling using different t_{bdry} . The resulting samples are drawn in blue color. The results show that a smaller t_{bdry} leads to a smaller clearance between contact samples and facet boundaries. (b) Results of contact sampling using different t_{rnn} . The resulting samples are drawn in red color. The results show that a smaller t_{rnn} leads to denser contact samples.

and smaller. In the extreme case where $\theta_{pln} = 0^\circ$, each triangle is treated as a facet.

Parameter 2: θ_{fct} is used to control the overlap of superimposed segmentation. Smaller θ_{fct} leads to more overlap between facets. Fig.13(b) shows the segmented results of the tube connector shown in Fig.12(a) using different θ_{fct} . Like Fig.13(a), each facet is drawn with a random offset and a random color. As θ_{fct} becomes smaller, facets become more overlapped.

Parameter 3: t_{bdry} is used to control the distance between

TABLE I: The tunable parameters

Name	Function	Where
θ_{pln}	Control the planarity of each facet	Appeared in superimpose segmentation
θ_{fct}	Control the overlap of facets	Appeared in superimpose segmentation
t_{bdry}	Control the distance between contacts and facet boundaries	Appeared in removing bad samples
t_{rnn}	Control the radius of contact regions	Appeared in removing bad samples
h_{max}	Control the stability of the planned grasps	Appeared in all grasp planners
θ_{parl}	Control the parallelity of two facets	Appeared in the planners for two and three-finger grippers
t_{dct}	Control the distances between finger pads and object surfaces	Appeared in the planner for three-finger grippers
n_{da}	The number of discretized rotation angles around contact normals	Appeared in all grasp planners

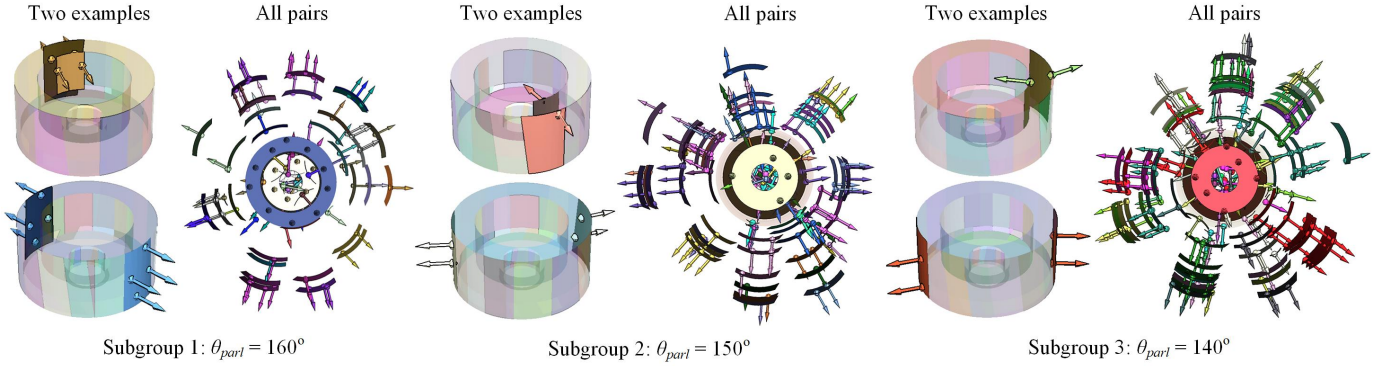


Fig. 15: Results of parallel facets using different θ_{parl} . Arrows indicate facet normals. Two facets with the same arrow color are parallel. The left part of each subgroup shows two exemplary pairs. The results show that as θ_{parl} decreases, less parallel facets are accepted. The right part of a subgroup shows all pairs. Here, the facets are drawn with random offsets from their original position to give a good view. As θ_{parl} decreases, more pairs are found.

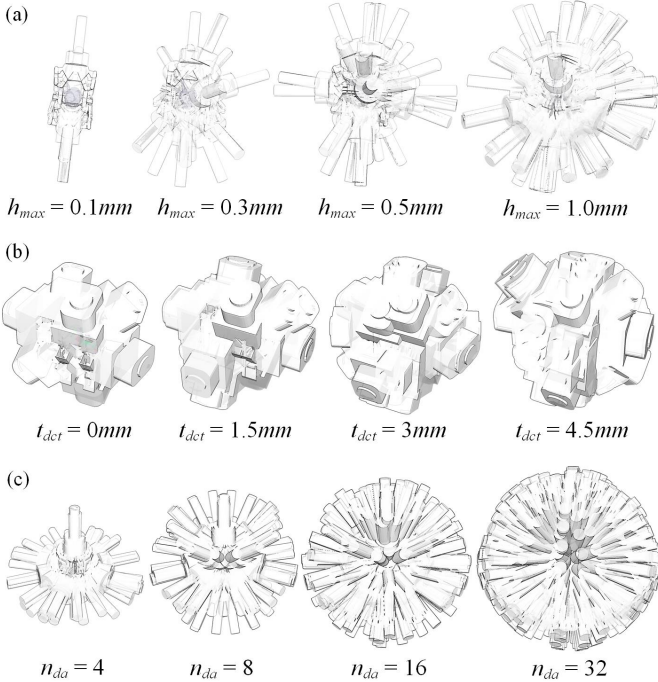


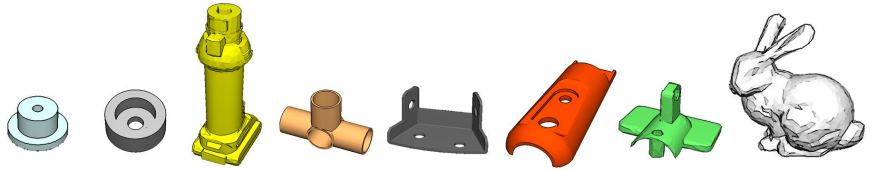
Fig. 16: (a) Results of grasp planning using different h_{max} . As h_{max} decreases, the hand grasps flat facets near the center of mass to maintain stability. Object: Stanford bunny, the last model in Fig.17. (b) Results of different t_{dct} . As t_{dct} increases, more grasps are found. Object: Tube connector, the fourth model in Fig.17. (c) Results of different n_{da} . A larger n_{da} leads to denser results. Object: Tube connector.

contacts and facet boundaries. Fig.14(a) shows the results of contact sampling using the metal workpiece shown in Fig.8(a) and different t_{bdry} . Only samples on the bottom of the object are drawn and the resulting samples are drawn in blue color. A smaller t_{bdry} leads to a smaller clearance between contact samples and facet boundaries (hence less robust results).

Parameter 4: t_{rnn} is used to control the radius of contact regions or the density of contact sampling. Fig.14(b) shows the sampling results of the metal workpiece using different t_{rnn} . The samples are drawn in red. A smaller t_{rnn} leads to denser contact samples on the object surface (hence more planned grasps).

Parameter 5: h_{max} is used to control the stability of the planned grasps. An example is shown in Fig.16(a). The object is the Stanford bunny (the last model in Fig.17). As h_{max} decreases, the planner reduces to grasp flat facets near the center of mass to maintain stability.

Parameter 6: θ_{parl} is used to control the parallelity of the facet pairs in the grasp planning. Values with a larger offset from 180° lead to more candidate “parallel” facet pairs to attach the finger pads and hence more planned grasps. On the other hand, values with larger offsets result in unstable grasping configurations. Fig.15 shows the parallel facets of a toy wheel using different θ_{parl} . Arrows indicate facet normals. Two facets with the same arrow color are parallel. Like Fig.13(a), the facets are drawn with random offsets from their original position to give a clear view. As θ_{parl} becomes smaller, “parallel” facets become less parallel. Meanwhile, the number of parallel facets becomes larger.



Information of mesh models	#vertices	362	468	1225	816	316	1390	893	1392
	#triangles	724	936	2441	1640	644	2786	1794	2780
Computational costs	Superimposed segmentation	0.154s	0.196s	0.936s	0.421s	0.137s	0.926s	0.509s	1.025s
	Sampling	0.050s	0.053s	0.095s	0.047s	0.038s	0.061s	0.067s	0.105s
	Remove bad samples 1	0.875s	1.281s	4.390s	1.993s	0.670s	6.805s	2.876s	5.586s
	Remove bad samples 2	0.020s	0.024s	0.063s	0.037s	0.012s	0.040s	0.025s	0.037s
	Plan contact pairs	0.144s	0.238s	1.634s	0.470s	0.051s	0.700s	0.208s	0.478s
	checkcollision(<i>stmesh</i> , <i>objmesh</i>)	0.236s	0.445s	0.142s	0.587s	0.104s	0.174s	0.179s	0.020s
	checkcollision(<i>eemesh</i> , <i>objmesh</i>)	2.445s	2.917s	5.691s	2.899s	2.843s	2.286s	9.091s	1.175s

Fig. 17: Computational cost of the proposed algorithms. The rows marked by red and blue shadows denote the most time consuming process. The values are the average results of ten executions using the following parameter setting: $\theta_{pln}=20^\circ$, $\theta_{fct}=20^\circ$, $t_{bdry}=2mm$, $t_{rnn}=3mm$, $t_{rss}=50mm$, $\theta_{part}=160^\circ$, $t_{dct}=3mm$, $n_{da}=8$.

Parameter 7: t_{dct} is used to control the distances between finger pads and object surfaces in the grasp planning for three-finger grippers. Larger values indicate the planner allows a large difference in distances between finger pads and object surfaces. In that case, there will be more planned grasps. Meanwhile, the results are less robust since two fingers cannot touch object surfaces at the same time. Fig.16(b) shows the planned grasps of the tube connector in Fig.12(b) using different t_{dct} . As t_{dct} becomes larger, the planned grasp configurations become denser. The object, which is obstructed by hands in the figure, is at the same pose as Fig.12(b). The results also show that when t_{dct} equals $0mm$, there are no lateral grasps. As t_{dct} becomes larger, the number of lateral grasps increase.

Parameter 8: In addition, n_{da} determines the number of discretized rotation angles around contact normals. A larger n_{da} leads to denser results, as is shown in Fig.16(c).

B. Performance

1) *Computational costs:* The computational costs of planning grasps for various objects using the method are shown in Fig.17. Six objects are used. From left to right, they are (1) a bearing housing, (2) a toy wheel, (3) an electric drill, (4) a tube connector, (5) a metal workpiece, and (6) a plastic workpiece. The information of these mesh models, including the number of vertices and the number of triangle faces, is shown in an upper section of the table in Fig.17. The details of computational cost, including the time spent on superimposed segmentation, sampling, removing bad samples 1 (refinement 1 of Fig.4), removing bad samples 2 (refinement 2 of Fig.4), planning contact pairs, and the two nested collision detection, are shown in a lower section of the table in Fig.17. The results are obtained by running the algorithms on a LENOVO ThinkPad P70 mobile workstation. One core of an Intel Xeon E3-1505M v5 @ 2.80GHz 4 Core CPU is used. The memory size is 16.0GB. The algorithms are implemented

using python 2.7.11 32 bit. The results are the average values of ten executions using the following parameter settings: $\theta_{pln}=20^\circ$, $\theta_{fct}=20^\circ$, $t_{bdry}=2mm$, $t_{rnn}=3mm$, $h_{max}=1.5mm$, $\theta_{part}=160^\circ$, $t_{dct}=3mm$, $n_{da}=8$.

The top two time-consuming rows are marked by red and blue shadows in Fig.4. The first one is checkcollision(*eemesh*, *objmesh*), which required a few seconds for a few thousand triangles. The results are reasonable as we are performing mesh-to-mesh collision detections. The second one is ‘‘Remove Bad Samples 1’’ (see Section III.B.2) and Fig.4). The cost is also reasonable since it measures the distances of each sampled contact point to the boundaries of facets.

2) *Influence of mesh quality:* Fig.18 shows the performance of the algorithms using a model with different mesh qualities. The meshes are drawn in Fig.18(1~8). The number of vertices and triangles of the meshes decreases from 1 to 8. The two charts in the figure show the normalized time cost and the normalized number of planned grasps on these models. Here, the maximum values are normalized as 1, the other values are normalized to values between 0 and 1. The maximum values are used as denominators for normalization. They are listed in the lower-left corner of the figure. In Chart (a), the different curves show the changes of various cost. The meanings of the colors are also shown in the lower-left corner. All curves in (a) are the results of the same parameter settings: $\theta_{pln}=20^\circ$, $\theta_{fct}=20^\circ$, $t_{bdry}=2mm$, $t_{rnn}=3mm$, $h_{max}=1.5mm$, $\theta_{part}=160^\circ$, $t_{dct}=3mm$, $n_{da}=8$. The two curves in Chart (b) show the number of planned grasps. The red curve is the changes of grasp number using the same parameter setting. The blue curve shows the results using a different θ_{part} value ($\theta_{part}=140^\circ$). The two curves show that the algorithms are stable to low-quality mesh models: The number of planned grasps does not significantly decrease along with reduced vertices and triangles. For $\theta_{part}=160^\circ$, the number of planned grasps is considered to have similar values in the red shadow

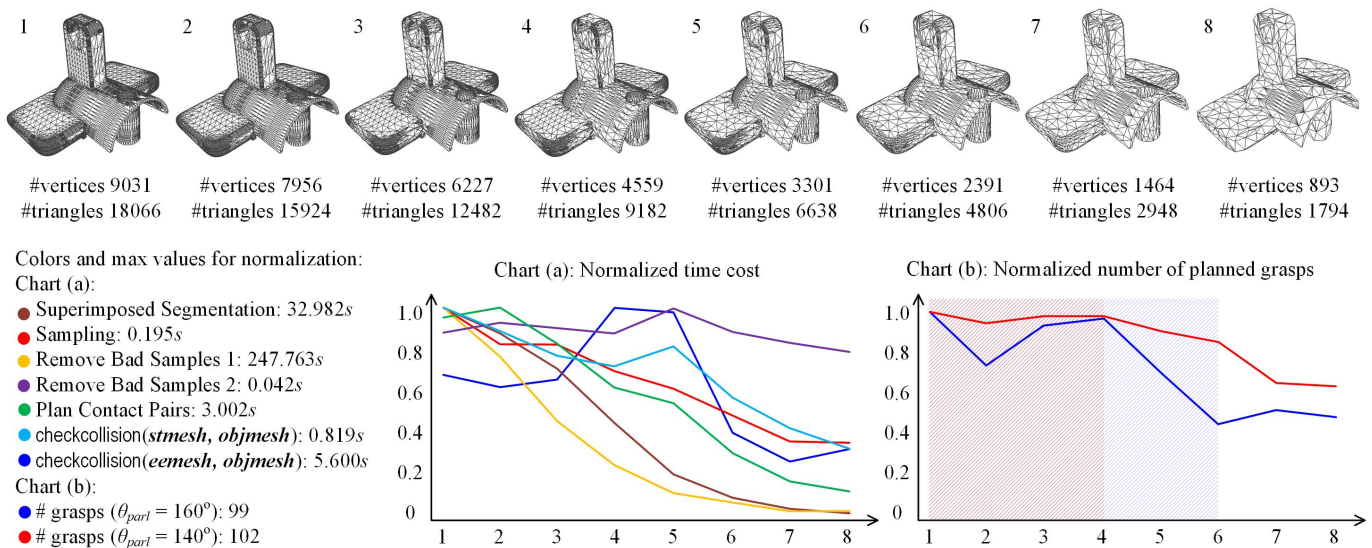


Fig. 18: Performance of the proposed algorithms using a model with decreasing mesh qualities. The meshes in 1~8 have a decreasing number of vertices and triangles and thus decreasing qualities. The curves in the two charts show the changes in time costs and the number of planned grasps as the mesh quality decreases.

(spans from 1 to 4). For $\theta_{parl}=140^\circ$, the number of planned grasps is considered to have similar values in the blue shadow (spans from 1 to 6).

3) *Precision of the planned grasps*: We further measure the precision of the planned grasps using a Robotiq85 two-finger parallel gripper and some objects. The experiment settings are shown in the right part of Fig.19. The objects include (a) the Stanford bunny, and (b) the bearing housing. AR markers are attached to the objects to precisely detect the changes of poses before and after closing the fingers. The grasps with approaching directions that have less than 40 degree angle from the vertical direction, as shown in the left part of Fig.19, are selected as the candidate grasps. They are used to grasp the objects. The difference in object poses (the difference in the AR marker's x and y positions, namely d_x and d_y) before and after grasping are measured as the precision.

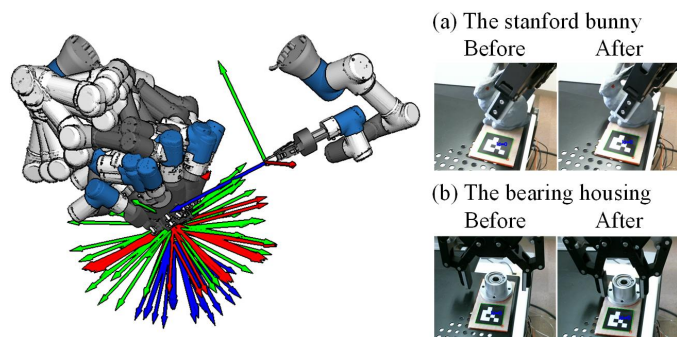


Fig. 19: Experimental settings used to examine the precision of the planned grasps. The left part shows the grasps with approaching directions that have less than 40° angle from the vertical direction. The changes in object poses before and after grasping are measured by AR markers shown in the right. Two objects, a Stanford bunny and a bearing housing, are tested.

The results of the Stanford bunny after grasping are shown in Fig.20. In the left case, θ_{parl} was set to 140° , and 6 candidate grasps were found. The maximum change after grasping using these planned grasps was $d_x=1.00mm$ and $d_y=4.50mm$. When θ_{parl} was changed to 160° (the right part of Fig.20), only 1 candidate grasp was found. Its change was $d_x=0.25mm$ and $d_y=1.00mm$.

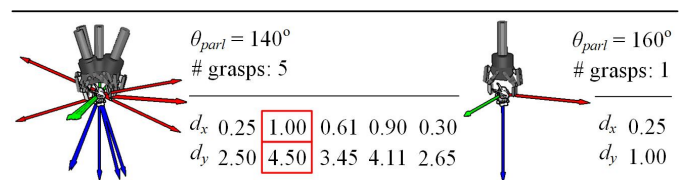


Fig. 20: Changes in positions after grasping the Stanford bunny using the planned grasps. The small 3D figures show the candidate grasps used for comparison. When $\theta_{parl}=140^\circ$, 6 candidate grasps are found. They are shown in the left 3D figure. When $\theta_{parl}=160^\circ$, only 1 candidate grasp is found. It is shown in the right 3D figure.

The Stanford bunny does not have many graspable parallel pairs. The available data might not be enough to demonstrate the precision of the planned grasps. Thus, we further examined the planned grasps of the bearing housing. The d_x and d_y before and after grasping the bearing housing using the planned grasps are shown in Fig.21. The first two rows of the table are the results using parameter settings: $\theta_{pln}=20^\circ$, $\theta_{fct}=20^\circ$, $t_{bdry}=2mm$, $t_{rnn}=3mm$, $h_{max}=1.5mm$, $\theta_{parl}=140^\circ$, $t_{dct}=3mm$, $n_{da}=8$. The lower two rows are the results using a different θ_{parl} . $\theta_{parl}=160^\circ$. When $\theta_{parl}=140^\circ$, there are 44 candidate grasps. Two failures are encountered during the experiments using these planned grasps. The failure cases are marked in red shadows. When $\theta_{parl}=160^\circ$, there are 32 candidate grasps, and all of them can successfully hold

$\theta_{parl} = 140^\circ$ # grasps: 44		d_x	1.25	0.50	0.00	2.00	77.00	1.75	0.63	0.25	1.63	0.37	2.00	2.11	1.68	2.19	1.86	1.59
		d_y	1.63	0.63	0.00	0.00	17.63	0.75	0.63	0.00	0.63	0.30	0.10	0.21	1.03	0.57	0.40	0.96
		d_x	1.44	0.42	0.26	0.57	0.03	0.28	0.44	0.52	0.61	79.00	0.52	0.03	0.55	0.24	1.70	1.33
		d_y	1.14	0.35	0.28	0.24	0.30	0.20	0.45	0.50	0.84	68.10	0.83	0.18	0.24	0.04	0.86	1.27
		d_x	1.67	1.55	1.62	1.89	1.15	2.06	1.49	1.96	0.68	0.38	0.71	0.52	-	-	-	-
		d_y	0.60	1.13	0.74	0.50	1.90	0.35	1.32	0.29	0.79	0.47	0.95	0.49	-	-	-	-
$\theta_{parl} = 160^\circ$ # grasps: 32		d_x	0.25	0.75	0.25	0.00	1.75	0.00	0.00	0.61	0.64	0.00	0.77	1.95	0.59	0.73	1.17	1.90
		d_y	1.37	1.63	1.88	0.00	0.00	0.00	0.00	1.62	1.92	0.78	1.50	1.16	0.00	0.00	0.01	0.00
		d_x	0.97	1.12	0.28	0.86	0.43	0.82	0.00	0.06	0.25	1.25	0.28	0.09	0.12	0.94	0.53	1.03
		d_y	0.08	0.37	0.01	0.27	1.43	1.17	1.47	1.02	0.00	0.00	0.23	1.27	1.39	1.26	0.00	0.00

Fig. 21: Changes in x and y after grasping the bearing housing using planned grasps. When $\theta_{parl}=140^\circ$, 44 candidate grasps were found. Their poses and precision are shown in the upper section of the table. The maximum positions change after grasping were $d_x=2.19mm$ and $d_y=1.90mm$. They are marked using red frames. Two failures were encountered when grasping using these planned grasps. They are marked using red shadows. When $\theta_{parl}=160^\circ$, 32 candidate grasps were found. Their poses and precision are shown in the lower section. The maximum changes were $d_x=1.95mm$ and $d_y=1.88mm$.

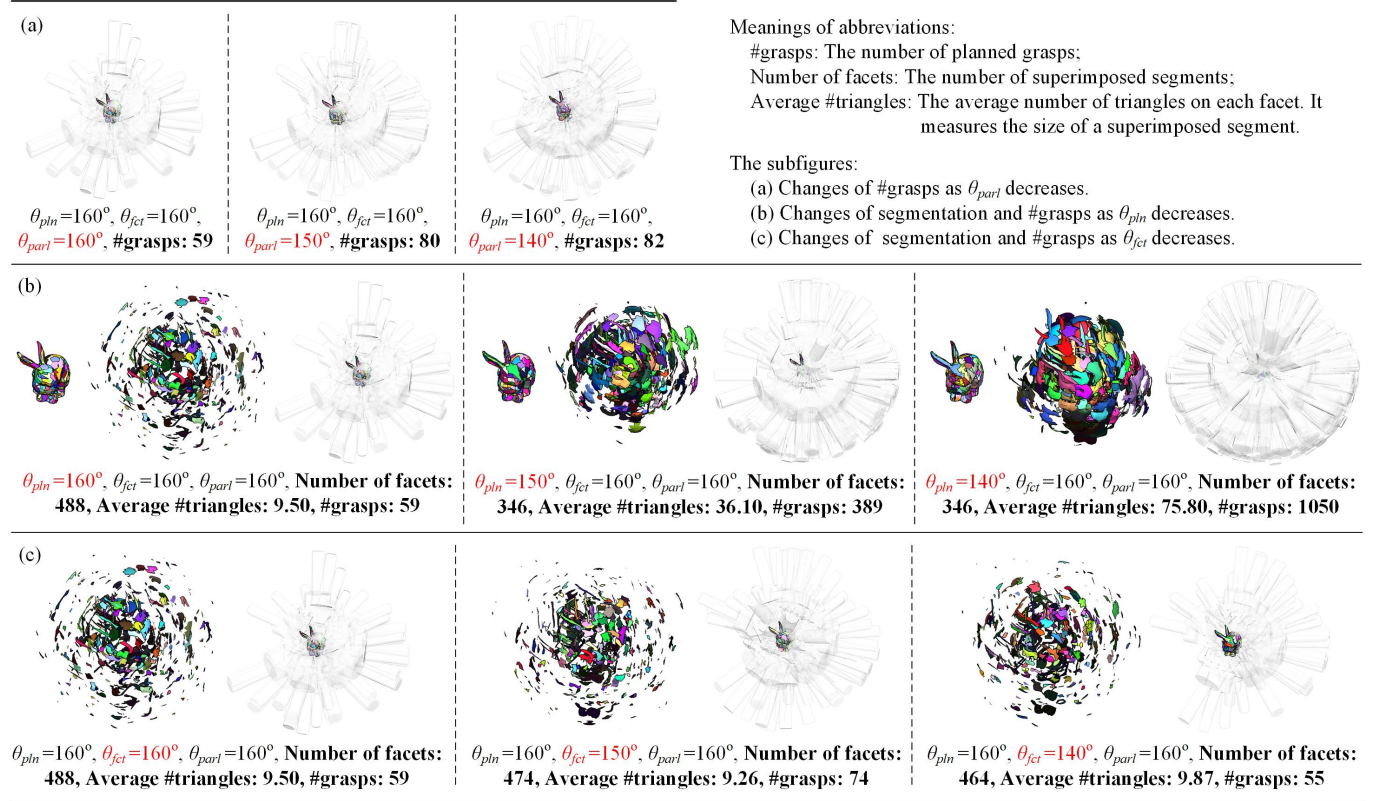


Fig. 22: Changes of segmentation and planned grasps of the stanford bunny with different parameter settings. The parameters included θ_{pln} , θ_{fct} , and θ_{parl} . At each row, two of these parameters are fixed to 160° , the left one decreases from left to right.

the object. The maximum position change after grasping are ($d_x=2.19mm$, $d_y=1.90mm$), and ($d_x=1.95mm$, $d_y=1.88mm$) in the two cases respectively. They are marked in red frames. With the results of these two models, we confirm that the planned grasps have satisfying precision and are suitable to be used by assembly routines (e.g. spiral search). Also, we may change the parameters of the algorithms and seek a balance between precision and the number of planned grasps according to the requirements of specific tasks (industrial bin-picking or assembly).

For readers' convenience, we summarize the detailed changes of segmentation and planned grasps of the Stanford bunny with different parameter settings in Fig.22. In (a), θ_{pln} and θ_{fct} are fixed to 160° , θ_{parl} decreases from left to right. The number of planned grasps increases as θ_{parl} decreases. In (b), θ_{fct} and θ_{parl} are fixed to 160° , θ_{pln} decreases from left to right. The sizes of facets increase significantly as θ_{pln} decreases (The sizes of facets are measured by the average number of triangles). Meanwhile, as the sizes of facets increases, the number of planned grasps increases significantly.

In (c), θ_{pln} and θ_{parl} are fixed to 160° , θ_{fct} decreases from left to right. The number of facets decreases slightly as θ_{fct} decreases. There are no necessary relations between θ_{fct} and the size of facets, and between θ_{fct} and the number of planned grasps.

C. Some robotic assembly examples using the grasp planner

The proposed method is implemented as a plugin of an open source project named PYHIRO (available on Github at <https://github.com/wanweiwei07/pyhiro>), where the goal is to build a system that conducts assembly tasks without human teach. The input to the system is the CAD models of objects and kinematic parameters of robots and hands. The output is a sequence of grasp configurations and robot poses for assembly. The proposed grasp planning is a pre-processing component of the project. It prepares pre-annotated grasp configurations for regrasp planning and motion planning. This subsection presents some examples of robotic assembly using the systems and the proposed grasp planning algorithms.

The first example is to use a Kawada Nextage robot (Kawada Industries, Inc.) to assemble a wheel to a support shown in Fig.23(a). The hands used were two Robotiq F-85 grippers. The input is the initial positions and orientations of the wheel and the support in a robot's workspace (the initial poses are shown in Fig.23(c)). The system automatically plans grasps, invalidates collided grasp configurations, and plans motion sequences using the collision-free grasps. The planned collision-free grasps for assembling the two objects are shown in Fig.23(b). Two exemplary planned sequences are shown in Fig.23(d.1) and (d.2). The real-world execution using one sequence is shown in Fig.23. The planned grasps are precise enough to guarantee successful pick-and-place and regrasp.

The second example is to use a dual-arm UR3 robot (Universal Robots A/S) to pick up a vacuum fastener and fasten a bolt. The robot plans a bunch of candidate grasps using the proposed algorithms, and chooses a suitable grasp to pick up the vacuum fastener in Fig.24(a-c). The planned grasp is precise enough to align the suction tooltip and fasten the bolt in Fig.24(d). Like the first example, the gripper used is the Robotiq F-85 gripper.

The third example is to hand over an electric drill from the right hand of an HRP5P robot (BNational Inst. of AIST, Japan, <http://y2u.be/ARpd5J5gDMk>) to its left hand. The gripper is a three-finger parallel gripper. The robot could precisely hold the object using the planned grasps (Fig.25(a-b)), which allows the left hand to insert its thumb into the narrow space between the index and middle fingers of the right hand Fig.25(c-d).

VI. CONCLUSIONS AND FUTURE WORK

In this paper, we proposed grasp synthesis algorithms that are efficient, have high precision, and are highly configurable with several tunable parameters. The algorithms focused on industrial end-effectors like grippers and suction cups, and can be used in industrial tasks like bin-picking and assembly. The efficiency, precision, and configurability of the proposed method meet the requirements of these tasks. The proposed

planner is demonstrated to be practical by a real-world robotic assembly task.

We envision our future research focusing on non-continuous contacts. In this paper, a finger pad is assumed to be continuously in contact with a flat surface of an object, which makes it difficult to find grasps on non-continuous surfaces, e.g. grasp the screw threads of a bolt. In the future, we will use surface simplification, reconstruction, and multi-contact analysis to plan grasps and challenge the difficulty.

REFERENCES

- [1] J. K. Salisbury, "Kinematic and Force Analysis of Articulated Hands," in *Robot Hands and the Mechanics of Manipulation*, pp. 2–167, The MIT Press, 1985.
- [2] B. Mishra, J. T. Schwartz, and M. Sharir, "On the Existence and Synthesis of Multifinger Positive Grips," *Algorithmica*, vol. 2, pp. 541–558, 1987.
- [3] V.-D. Nguyen, "Constructing Force-Closure Grasps," in *Proceedings of IEEE International Conference on Robotics and Automation*, pp. 1368–1373, 1986.
- [4] Y. Funahashi, T. Yamada, M. Tate, and Y. Suzuki, "Grasp Stability Analysis Considering the Curvatures at Contact Points," in *Proceedings of IEEE International Conference on Robotics and Automation*, pp. 3040–3046, 1996.
- [5] E. Rimon and J. W. Burdick, "Mobility of Bodies in Contact – I: A New 2nd Order Mobility Index for Multiple-Finger Grasps," *IEEE Transactions on Robotics and Automation*, vol. 14, pp. 696–708, 1998.
- [6] Yun-Hui Liu, "Computing n-Finger Form-Closure Grasps on Polygonal Objects," *The International Journal of Robotics Research*, vol. 19, no. 2, pp. 149–158, 2000.
- [7] A. F. van der Stappen, "Immobilization: Analysis, Existence, and Output-sensitive synthesis," in *Computer-Aided Design and Manufacturing*, pp. 162–187, AMS-DIMACS, 2005.
- [8] D. J. Montagna, "The Condition for Contact Grasp Stability," in *Proceedings of IEEE International Conference on Robotics and Automation*, pp. 412–417, 1991.
- [9] A. Bicchi, "On the Closure Properties of Grasping," *The International Journal of Robotics Research*, vol. 14, pp. 319–334, 1995.
- [10] W. S. Howard and V. Kumar, "On the Stability of Grasped Objects," *IEEE Transactions on Robotics and Automation*, 1996.
- [11] B. Mishra, "Grasp metrics: Optimality and Complexity," in *Proceedings of Workshop on Algorithmic Foundations of Robotics*, pp. 137–165, 1995.
- [12] M. A. Roa and R. Suárez, "Grasp Quality Measures: Review and Performance," *Journal of Autonomous Robots*, vol. 38, pp. 65–88, 2015.
- [13] J. Ponce, S. Sullivan, A. Sudsang, and J. Merlet, "On Computing Four-finger Equilibrium and Force-closure grasps of Polyhedral Objects," *IEEE Transactions on Robotics and Automation*, vol. 16, pp. 11–35, 1997.
- [14] Y. Liu, M. Lam, and D. Ding, "A Complete and Efficient Algorithm for Searching 3-D Form Closure Grasps in the Discrete Domain," *IEEE Transactions on Robotics and Automation*, vol. 20, pp. 805–816, 2004.
- [15] M. Fischer and G. Hirzinger, "Fast Planning of Precision Grasps for 3D Objects," in *Proceedings of IEEE/RSJ International Conference on Intelligent Robots and Systems*, pp. 120–126, 1997.
- [16] A. Miller and P. Allen, "Examples of 3D Grasp Quality Computations," in *Proceedings of IEEE International Conference on Robotics and Automation*, pp. 1240–1246, 1997.
- [17] J. D. Wolter, R. A. Volz, and A. C. Woo, "Automatic Generation of Gripping Positions," *IEEE Transactions on System, Man, and Cybernetics*, vol. 15, pp. 204–213, 1985.
- [18] J. L. Jones and T. Lozano-Perez, "Planning Two-Fingered Grasps for Pick-and-Place Operations on Polyhedra," in *IEEE International Conference on Robotics and Automation*, pp. 683–687, 1990.
- [19] C. Liu, H. Qiao, J. Su, and P. Zhang, "Vision-Based 3-D Grasping of 3-D Objects With a Simple 2-D Gripper," *IEEE Trans. Systems, Man, and Cybernetics: Systems*, vol. 44, no. 5, pp. 605–620, 2014.
- [20] M. Pozzi, M. Malvezzi, and D. Prattichizzo, "On Grasp Quality Measures: Grasp Robustness and Contact Force Distribution in Underactuated and Compliant Robotic Hands," *IEEE Robotics and Automation Letters*, vol. 2, no. 1, pp. 329–336, 2017.

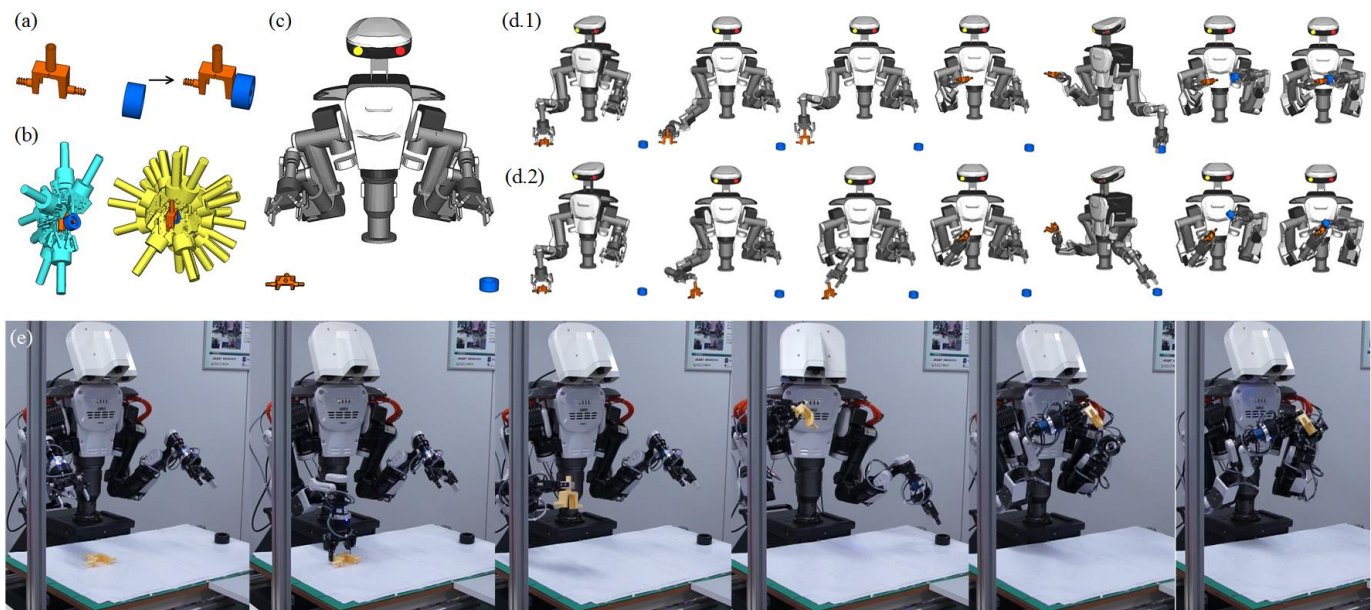


Fig. 23: Using a Kawada Nextage robot to conduct an assembly task. (a) The goal of the assembly task. (b) The planned collision-free grasps for assembly. The cyan hands show the possible grasp configurations to hold the support. The yellow hands show the possible grasp configurations to hold the wheel. (c) The initial poses of the objects to be assembled. (d) Two exemplary planned sequences using the planned grasps. (e) A real-world execution.

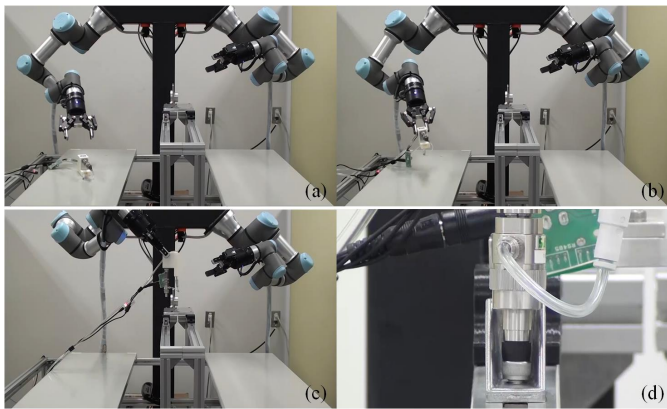


Fig. 24: Using a dual-arm UR3 robot to pick up a vacuum fastener and fasten a bolt. (a-c) The robot chooses a suitable grasp from preplanned grasps to pick up the vacuum fastener. (d) The planned grasp is precise enough to align the suction tooltip and fasten the bolt.

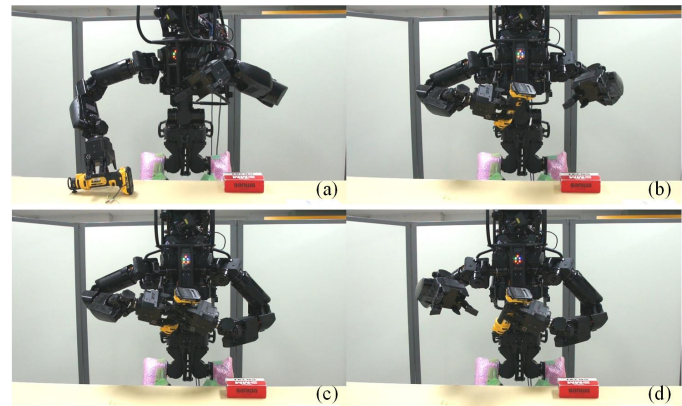


Fig. 25: Handing over a tool driver from the right hand of an HRP5P robot to its left hand. (a-b) The robot picks up the electric drill using its left hand and prepares it for handover. (c) Handover. The right hand inserted its thumb into the narrow space between the index and middle fingers of the right hand to hold the drill. (d) The left hand released and the object is successfully delivered.

- [21] J. Shi and G. S. Koonjul, "Real-Time Grasping Planning for Robotic Bin-Picking and Kitting Applications," *IEEE Transactions on Automation Science and Engineering*, vol. 14, no. 2, pp. 809–819, 2017.
- [22] Y. Li, J. P. Saut, J. Pettr, A. Sahbani, and F. Multon, "Fast Grasp Planning Using Cord Geometry," *IEEE Transactions on Robotics*, vol. 31, no. 6, pp. 1393–1403, 2015.
- [23] M. Ciocarlie, C. Lackner, and P. Allen, "Soft Finger Model with Adaptive Contact Geometry for Grasping and Manipulation Tasks," in *Proceedings of Joint EuroHaptics Conference and Symposium on Haptic Interfaces for Virtual Environment and Teleoperator Systems*, pp. 219–224, 2007.
- [24] K. Harada, T. Tsuji, K. Nagata, N. Yamanobe, K. Maruyama, A. Nakamura, and Y. Kawai, "Grasp Planning for Parallel Grippers with Flexibility on Its Grasping Surface," in *Proceedings of IEEE International Conference on Robotics and Biomimetics*, pp. 1540–1546, 2011.
- [25] C. Goldfeder, P. K. Allen, C. Lackner, and R. Pelosoff, "Grasp Plan-

- ning via Decomposition Trees," in *Proceedings of IEEE International Conference on Robotics and Automation*, pp. 4679–4684, 2007.
- [26] H. Zha, T. Hoshida, and T. Hasegawa, "A recursive Fitting-and-splitting Algorithm for 3-D Object Modeling using Superquadrics," in *Proceedings of International Conference on Pattern Recognition*, pp. 658–662, 1998.
- [27] S. El-Khoury, A. Sahbani, and V. Perdereau, "Learning the Natural Grasping Component," in *Proceedings of IEEE/RSJ International Conference on Intelligent Robots and Systems*, pp. 2957–2962, 2007.
- [28] Z. Xue, A. Kasper, J. M. Zoellner, and R. Dillmann, "An Automatic Grasp Planning System for Service Robots," in *Proceedings of International Conference on Advanced Robotics*, pp. 1–6, 2009.
- [29] A. T. Miller, S. Knoop, H. I. Christensen, and P. K. Allen, "Automatic

- Grasp Planning Using Shape Primitives,” in *Proceedings of IEEE International Conference on Robotics and Automation*, pp. 1824–1829, 2003.
- [30] K. Huebner, S. Ruthotto, and D. Kragic, “Minimum Volume Bounding Box Decomposition for Shape Approximation in Robot Grasping,” in *Proceedings of IEEE International Conference on Robotics and Automation*, pp. 1628–1633, 2008.
- [31] M. Bonilla, D. Resasco, M. Gabiccini, and A. Bicchi, “Grasp Planning with Soft Hands using Bounding Box Object Decomposition,” in *Proceedings of International Conference on Intelligent Robots and Systems*, pp. 518–523, 2015.
- [32] K. Nagata, T. Miyasaka, D. N. Nenchev, N. Yamanobe, K. Maruyama, S. Kawabata, and Y. Kawai, “Picking up An Indicated Object in a Complex Environment,” in *Proceedings of IEEE/RSJ International Conference on Intelligent Robots and Systems*, pp. 2109–2116, 2010.
- [33] N. Yamanobe and K. Nagata, “Grasp Planning for Everyday Objects Based on Primitive Shape Representation for Parallel Jaw Grippers,” in *Proceedings of IEEE International Conference on Robotics and Biomimetics*, pp. 1565–1570, 2010.
- [34] N. Curtis and J. Xiao, “Efficient and Effective Grasping of Novel Objects through Learning and Adapting a Knowledge Base,” in *Proceedings of IEEE/RSJ International Conference on Intelligent Robots and Systems*, pp. 2252–2257, 2008.
- [35] K. Harada, K. Nagata, T. Tsuji, N. Yamanobe, A. Nakamura, and Y. Kawai, “Probabilistic Approach for Object Bin Picking Approximated by Cylinders,” in *Proceedings of IEEE International Conference on Robotics and Automation*, pp. 3727–3732, 2013.
- [36] F. T. Pokorny, K. Hang, and D. Kragic, “Grasp Moduli Spaces,” in *Proceedings of Robotics: Science and Systems*, 2013.
- [37] T. Tsuji, S. Uto, K. Harada, R. Kurazume, T. Hasegawa, and K. Morooka, “Grasp Planning for Constricted Parts of Objects Approximated with Quadric Surfaces,” in *Proceedings of IEEE/RSJ International Conference on Intelligent Robots and Systems*, pp. 2447–2453, 2014.
- [38] M. Garland, A. Willmott, and P. S. Heckbert, “Hierarchical Face Clustering on Polygonal Surfaces,” in *Proceedings of Symposium on Interactive 3D Graphics*, pp. 49–58, 2001.
- [39] K. Hang, J. A. Stork, F. T. Pokorny, and D. Kragic, “Combinatorial Optimization for Hierarchical Contact-level Grasping,” in *Proceedings of IEEE International Conference on Robotics and Automation*, pp. 381–388, 2014.
- [40] K. Hang, J. A. Stork, and D. Kragic, “Hierarchical Fingertip Space for Multi-fingered Precision Grasping,” in *Proceedings of IEEE/RSJ International Conference on Intelligent Robots and Systems*, pp. 1641–1648, 2014.
- [41] K. Hang, M. Li, J. A. Stork, Y. Bekiroglu, F. T. Pokorny, A. Billard, and D. Kragic, “Hierarchical Fingertip Space: A Unified Framework for Grasp Planning and In-Hand Grasp Adaptation,” *IEEE Transactions on Robotics*, vol. 32, no. 4, pp. 960–972, 2016.
- [42] Y. Zhang, A. Koschan, and M. Abidi, “Superquadrics Based 3D Object Representation of Automotive Parts Utilizing Part Decomposition,” in *Proceedings of International Conference on Quality Control by Artificial Vision*, pp. 241–251, 2003.
- [43] A. D. Kalvin and R. H. Taylor, “Superfaces: Polygonal Mesh Simplification with Bounded Error,” *IEEE Computer Graphics and Applications*, vol. 16, no. 3, pp. 64–77, 1996.
- [44] K. Harada, T. Tsuji, S. Uto, N. Yamanobe, K. Nagata, and K. Kitagaki, “Stability of soft-finger grasp under gravity,” in *Proceedings of IEEE International Conference on Robotics and Automation (ICRA)*, pp. 883–888, 2014.
- [45] W. Wan and K. Harada, “Developing and Comparing Single-arm and Dual-arm Regrasp,” *IEEE Robotics and Automation Letters*, pp. 243–250, 2016.
- [46] W. Wan and K. Harada, “Integrated Assembly and Motion planning using Regrasp Graphs,” *Robotics and Biomimetics*, vol. 3:18, 2016.
- [47] W. Wan and K. Harada, “Achieving High Success Rate in Dual-arm Handover Using Large Number of Candidate Grasps,” *Advanced Robotics*, pp. 1111–1125, 2016.
- [48] W. Wan and K. Harada, “Regrasp Planning using 10,000 Grasps,” in *Proceedings of IEEE/RSJ International Conference on Intelligent Robots and Systems*, pp. –, 2017.